sustainability

MDPI

Article

Experimental Study on the Movement of Boulders in Debris Flow: Influence of Boulder Size and Initial Orientation

Rendong Liu [1], Fei Wang [1,*], Jiading Wang [1], Xiaoqing Chen [2], Haijun Qiu [3] and Canyun Lou [1]

[1] State Key Laboratory of Continental Dynamics, Department of Geology, Northwest University, Xi'an 710069, China; liurendong188@163.com (R.L.); wangjd@nwu.edu.cn (J.W.); lou_cy2022@163.com (C.L.)
[2] CAS Key Laboratory of Mountain Hazards and Earth Surface Process, Institute of Mountain Hazards and Environment, Chinese Academy of Sciences, Chengdu 610041, China; xqchen@imde.ac.cn
[3] Shaanxi Key Laboratory of Earth Surface System and Environmental Carrying Capacity, Institute of Earth Surface System and Hazards, College of Urban and Environmental Sciences, Northwest University, Xi'an 710127, China; haijunqiu@nwu.edu.cn
* Correspondence: wf@nwu.edu.cn

Abstract: In debris-flow disasters, boulders moving at high velocities cause significant damage to houses and other facilities. Through a flume model test, this study explored the influences of the length/width ratio of the boulders, the angle between the long axis of the boulders and the flow direction, and the density of the mudflow on their starting movement. The experimental results indicate that in the process of a mudflow impacting the boulders, the angle between the long axis and the flow direction influences the magnitude of the component forces of the dragging force in the long- and short-axis directions, thus causing the boulders to deviate. Deflection changes the area of action of the debris-flow drag force on the boulder. Once the boulder gains a certain velocity, it deviates toward a state in which the long axis is parallel to the flow direction to reduce the resistance in the movement process. When the long axis of the boulder is parallel to the flow direction, as the mass of the boulder decreases, the efficiency of the mudflow in transferring the velocity of the boulder increases. When there is an angle between the long axis of the boulder and the flow direction, as the angle increases, the area of the drag force and efficiency of the velocity transfer increase. The movement laws of boulders in mudflows are crucial for engineering construction and sustainable development in mountainous areas.

Keywords: mudflow; boulder; length/width ratio; drag force; flume experiment; sustainable development

check for updates

Academic Editor: Gerardo Araya-Letelier

Received: 2 December 2024
Revised: 23 December 2024
Accepted: 27 December 2024
Published: 29 December 2024

Citation: Liu, R.; Wang, F.; Wang, J.; Chen, X.; Qiu, H.; Lou, C. Experimental Study on the Movement of Boulders in Debris Flow: Influence of Boulder Size and Initial Orientation. *Sustainability* **2025**, *17*, 179. https://doi.org/10.3390/su17010179

Copyright: © 2024 by the authors. Licensee MDPI, Basel, Switzerland. This article is an open access article distributed under the terms and conditions of the Creative Commons Attribution (CC BY) license (https://creativecommons.org/licenses/by/4.0/).

1. Introduction

Debris flows often move at high speeds along valleys, exhibiting suddenness, transience, and powerful impact forces. Every year, debris flow disasters in mountainous regions cause significant damage to infrastructure, property loss, and casualties [1–3]. The major hazards of debris flows include scouring, siltation, and impact damage, with the most severe consequence being impact damage [4]. Boulders carried by debris flows can inflict severe damage to towns, railroads, bridges, and other facilities downstream of the gullies. For example, on 9 July 1981, on the Chengkun Railroad in Ganluo County, Sichuan Province, a large debris flow occurred in the Lizi Yida Gully on the Dadu River that destroyed the bridge abutment, resulting in an accident that killed more than 400 people [5]. On 11 August 2023, a debris flow broke out in the Jiwozi group in Chang'an District, Xi'an City, Shaanxi Province, and boulders carried by the debris flow impacted houses and roads

at the gully's entrance, leading to the deaths of more than 40 people and considerable damage. Additionally, boulders also appeared in the Aizigou debris flow and the Xiaogangjian debris flow in Sichuan, China. Figure 1 shows the boulders used in debris flow disasters in Sichuan and Shaanxi, China.



(**a**) Aizigou Debris flow, Sichuan Province, China



(**b**) Xiaogangjian Debris flow, Sichuan Province, China



(**c**) Jiwozi Debris flow, Shaanxi Province, China

Figure 1. Boulders at the debris flow scene.

Numerous studies have been conducted on the impact characteristics of debris flows [6–9]. Relatively few studies have been conducted on the initiation, movement, and impact force of boulders under the action of debris flows. The boulders in the debris flow are jointly affected by many factors, such as buoyancy, friction, impact force between the boulders, and the dynamic pressure of the debris flow, which includes forms such as rolling, sliding, and bouncing. Many influencing factors have complex three-dimensional (3D) movement characteristics [5]. As the destructive power of boulders in debris flows is extremely strong, research on the movement characteristics of boulders in debris flows has guiding significance for disaster prevention and reduction projects for mountainous debris flows.

Currently, there is relatively little research on the movement of boulders during debris flow disasters. Numerical simulation calculations and theoretical analyses are mainly used to study the movement of boulders. Xu established model equations for the motion of large particles in a debris flow by analyzing the forces between the particles in a debris flow, as well as the forces between the particles, debris flow, and riverbed [10]. Wang used FLOW-3D to establish a boulder collision model after silting a sand barrage and investigated the rolling characteristics of the boulders under a three-dimensional turbulence model [5]. Tang and Sun investigated the relationship between the initiation of large particles in debris flows and water flow conditions [11]. Using the concept of probability theory to solve

the problem of random distribution of particles on slopes, he solved moment balance equations for the critical initiation of large particles. Tang established a reasonable and concise calculation model for the initiation of large particles in viscous debris flows [12]. Si found that the irregular shape of a boulder significantly affects its impact [13]. Vicari used numerical simulation techniques to simulate boulder impacts on gullies and debris flows that reduced the mobility of debris flows [14]. Wang researched the movement and sedimentary characteristics of boulders in debris flow using a fluid-solid coupling model that simulated the change rules of the center-of-mass velocity, angular velocity, and kinetic energy of boulders in different periods [15]. Sha proposed a procedure for evaluating the impact force of a debris flow on an obstacle by combining simulation methods of the debris flow transport of boulders and CEL [16]. It mainly uses numerical simulation techniques to study the critical conditions for boulder initiation, the impact of boulders on the flow characteristics of debris flows, the analysis of boulder impact force, and so on. There have been few modeling experiments on boulder movement, and numerical simulation techniques have some limitations.

Research on the movement of boulders in debris flows can be inspired by studies on the movement of objects, such as boulders, containers, vehicles, and boats, on the shore caused by storms or tsunamis. Nott developed hydrodynamic equations for evaluating the wave characteristics required for the transport of coastal boulders triggered by tsunamis or storms, and these equations have been widely cited and used [17,18]. Many scholars have analyzed the motion of boulders under the action of tsunami waves by employing three-dimensional (3D) fluid dynamics coupled with rigid body dynamics to simulate the study [18–23]. In addition to the shape, size, and density of boulders, the environment in which coastal boulders are transported determines the wave heights required to move them [18]. Goto suggested that boulders carried by tsunamis are typically deposited below the high tide line [19]. Paris studied the morphology and distribution of coastal boulders and estimated the size of movable particles using the simulated flow velocity of tsunami waves to deduce the movement of finer sediments in the coastal ocean [20]. The results showed that the spatial distribution, particle size distribution, and source of boulders on the coast were controlled by the initial distribution of boulders, hydrodynamic characteristics of the tsunami, and topography. Numerical models can simulate the wave flow velocity, particle size range of moving particles, and wave-breaking height required for boulder movement. However, there are always differences between simulation and reality, and there are still some unknown parameters that can affect the accuracy of the numerical model.

Other scholars have conducted flume experiments to study the boulder transportation process under tsunami action using equal-scale boulder models [24–28]. Imamura suggested that boulders are mainly carried under tsunami action by rolling or jumping rather than sliding [24]. Bressan investigated the critical relationship among the mass, geometry, location, flow velocity, and flow depth of boulders when initiated [25]. Liu suggested that the movement of boulders is mainly divided into three phases: acceleration, deceleration, and relatively stable movement [26]. Oetjen experimented with real boulders to simulate waves on three shore types [27]. In comparison to numerical simulation techniques, physical modeling experiments can visualize the real situation of boulder movement, but the experiments are subject to many errors owing to human manipulation; therefore, a large number of experiments need to be conducted to minimize the effects of errors. Research on the stability of automobiles in floods can provide ideas and methods for studying boulder movement in debris flows as well [29–31]. Xiao analyzed the force on a car in a partially submerged state in a flood based on the sediment initiation theory to derive a formula for the initiation flow rate of a car in a flood [29]. In the research fields of tsunami-carrying

boulders and flood-impacting vehicles, scholars have primarily focused on boulder size, density, shape, and wave characteristics.

This study focuses on rectangular boulders to investigate the effects of loess mudflow density, boulder length/width ratio, and the initial angle between the long axis of the boulder and the direction of the mudflow on its initiation velocity, movement distance, and movement form. The results of these studies can provide references for studies on the initiation and movement of boulders in mudflows, calculation of boulder impact force, and risk assessment. It is of vital importance to the engineering construction and sustainable development in mountainous areas.

2. Materials and Methods

2.1. Experimental Setup

The experiment device consists of three parts: a water tank for storing and releasing pre-configured mudflow, a tailings pond located below the flume to collect debris-flow waste, and a flume for simulating the interaction with boulders during mudflow movement. The flume is 8.5 m long, 0.45 m wide, and 0.5 m deep, made of steel plate at the bottom and transparent toughened glass at the two sides. At the junction between the tank and the channel, there is a rectangular sluice gate, which is used to release the mudflow. The volume of the tailings pond was 1.2 m^3, and the inclination angle of the flume was 9°. A laser sensor (Leuze, Owen, Germany, ODSL, at a rate of 10 Hz, named laser) and three cameras (Canon LEGRIA with resolutions of 1440 × 1080 pixels and frame rates of 25 frames per second (fps), named cameras 1, 2, and 3) were used in the experiment. A laser rangefinder was placed upstream of the boulder to monitor changes in the mud depth and the mudflow in the flume during the test. Camera 1 was placed above the boulder to monitor the motion characteristics of the boulder model. Camera 2 was placed downstream of the flume to record the possible motions of the boulder (sliding, deflection, rolling, bouncing). Camera 3 was located at the side of the flume to record the boulder's motion. The experimental setup is illustrated in Figure 2.

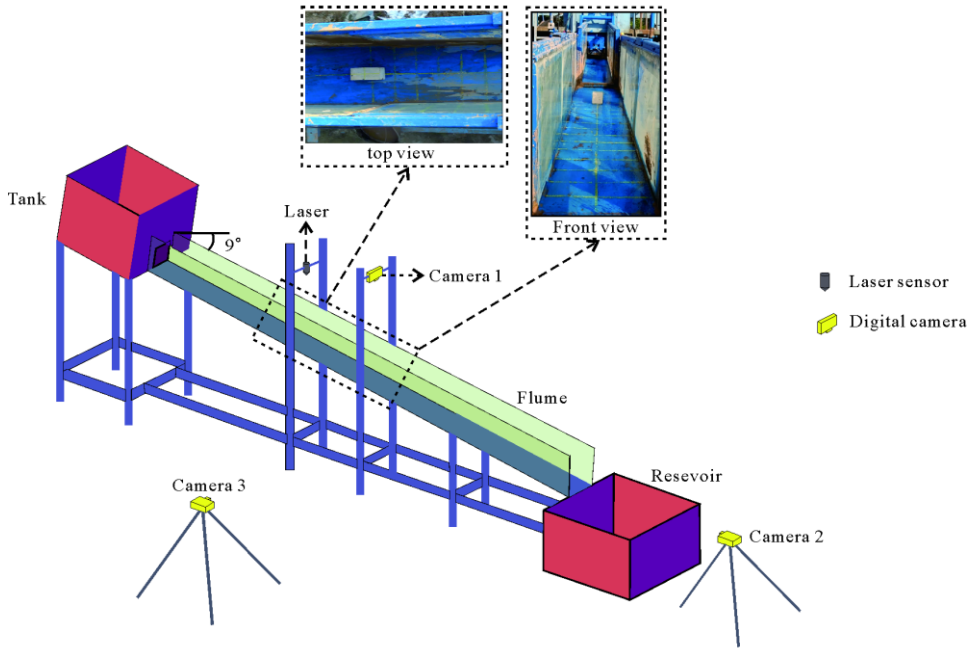


Figure 2. Experimental setup diagram.

2.2. Test Material

The soil used to prepare the mudflow was obtained from Baoji City, Shaanxi Province, China, with a natural moisture content of approximately 18.7%, a density of 1.63 g/cm^3, and a dry density of 1.37 g/cm^3. The loess had a particle size of 0.05 mm for d_{85}, 0.025 mm for d_{60}, and 0.008 mm for d_{30}. The distribution of the soil particle sizes is shown in Figure 3.

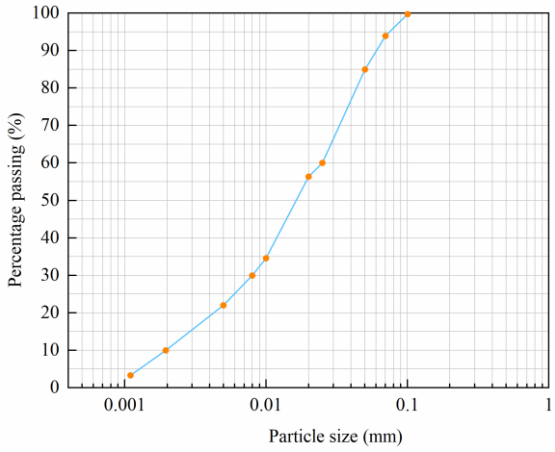


Figure 3. Particle size diagram of the experiment soil.

The required density of the mudflow is configured according to the experimental scheme, and an electric mixer is used to make it uniform to reduce the phenomenon of solid particle agglomeration and precipitation; thus, the motion characteristics of the configured mudflow are more in line with reality. The configuration of the mudflow and mixing operation are shown in Figure 4.



Figure 4. (**a**) Pre-configured mudflow. (**b**) Mix the mudflow.

2.3. Boulder Models

In the experiment, four boulder models were created by pouring concrete into pre-made plastic molds. The height and width of the four boulder models are the same (8 cm), and the difference lies in the length/width ratio (n), $n = a/b$, where a, b, and c refer to the length, width, and height of the boulders, respectively. The dimensions and physical objects of the boulder model are shown in Figure 5. In the research on the movement of the boulders under the effect of the tsunami, $(a + b)/2c$ was used to indicate the flatness indexes of the boulders, which were used to classify boulders of different sizes [32]; however, because only the long axis dimensions were changed in this experiment, to respond more clearly to the effect of the length change, the n of the boulder models were used to classify the boulders. The n values of boulder models 1, 2, 3, and 4 were 2, 1.625, 1.375, and 1.

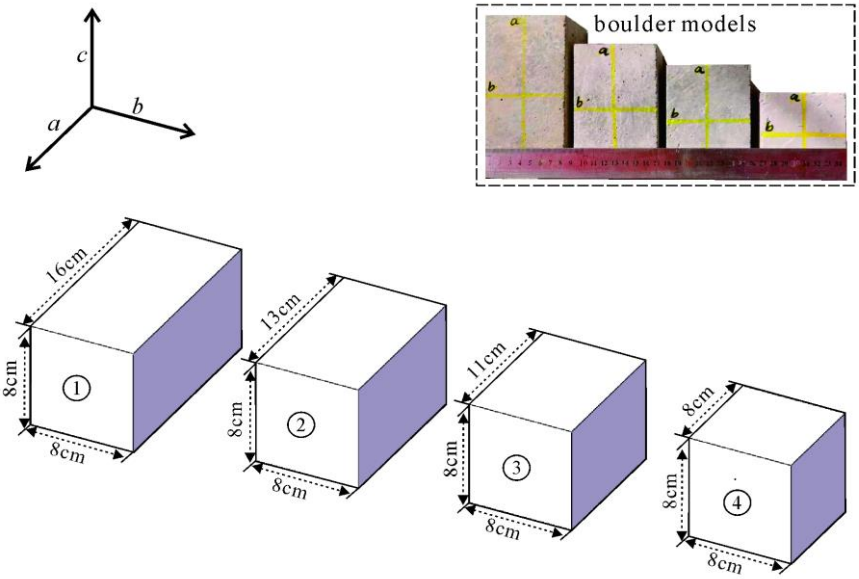


Figure 5. Characteristics and objects of the boulder model. a, b, and c refer to the length, width, and height of the boulders, respectively. The n values of boulder models 1, 2, 3, and 4 were 2, 1.625, 1.375, and 1.

2.4. Experimental Scale

Because the flow characteristics of debris flows are very complex, to make the debris flow in the experiment configured closer to the natural debris flow state, the debris flow configured in the experiment and the natural debris flow should follow the gravity similarity (Froude) criterion [33]. The Froude number (F_r) is a dimensionless parameter used to characterize the relative magnitudes of fluid inertial forces and gravity. F_r as expressed in Equation (1) [34,35]. The F_r of the debris flows configured in the experiment ranged from 4.53 to 6.39, which is in the range of the Froude number for normal debris flows, making this experiment feasible.

$$F_r = \frac{v}{\sqrt{gh\cos\theta}} \tag{1}$$

In the formula, v is the debris flow velocity (m/s), h is the debris flow depth (m), g is the gravity acceleration (m/s^2), and θ is the slope of the flume (°).

In the experiment, the boulder model made of concrete pouring is used to simulate the boulders in the mudflow event, and the given length scale (λ_L) is shown as in Equation (2). According to the gravity similarity criterion, the velocity scale (λ_V) is as shown in Equation (3) [36–38]. The experimental scale set was 1:50, and the four boulder models simulated boulders with widths and heights of 4 m and, respectively, 4 m, 5.5 m, 6.5, and 8 m.

$$\lambda_L = 1:50 \tag{2}$$

$$\lambda_V = \lambda_L^{0.5} = 1:7.1 \tag{3}$$

2.5. Experiment Design

The experiments were divided into two groups to investigate the effects of the length/width ratio of the boulder, the angle between the long axis and flow direction, and the density of the mudflow on the movement of the boulder. In test one, the long axis of the boulder was parallel to the flow direction, controlling for changes in the length/width ratio of the boulder and the density of the mudflow. In Test 2, the length/width ratio of the boulder was 2, controlling for variations in the angle of the long axis of the boulder with the flow direction, as well as for variations in the density of the mudflow.

The complexity of field conditions, with different source conditions in different areas and different rainfall conditions, makes the density of mudflows very different. The movements of boulders under different types of mudflows are also different. To simulate the movement of boulders in floods, dilute mudflow, and neutral mudflow, we set up floods with a density of 1000 kg/m^3 and mudflows with densities of 1150 kg/m^3, 1300 kg/m^3, and 1450 kg/m^3.

The sizes of boulders are often different, and boulders with different length/width ratios have different motions under the impact of mudflows. Therefore, four boulder models with different length-to-width ratios were used to simulate the effect of the length-to-width ratio of boulders on boulder movement in Test 1, and the length/width ratio of the four types of boulders were 2, 1.625, 1.375, and 1, respectively.

The initial positions of the boulders in the channel were different, and the angle between the long axis of the rectangular boulder and the direction of the mudflow was related to the magnitude of the impact force received by the boulder from the mudflow. Four different angles of 0°, 33.3°, 66.6°, and 90° were set for the angle between the long axis of the boulder and flow direction in Test 2.

The position of the boulder model in the sink is illustrated in Figure 6. Each test was performed 16 times, for a total of 32 times. The experimental parameters are listed in Table 1.

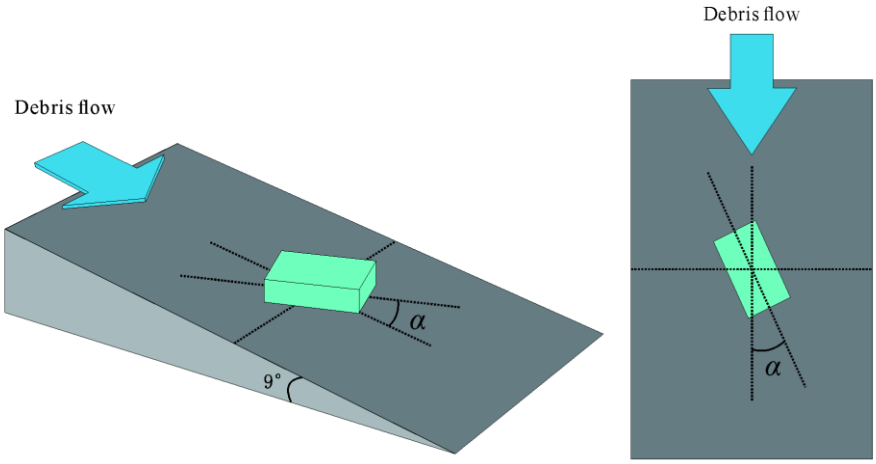


Figure 6. The position of the boulder model in the flume. α is the angle between the long axis of the boulder and the flow direction of the debris flow.

Table 1. Experimental variables.

	V (m^3)	n	α (°)	ρ (kg/m^3)
Test 1	0.05	1	0	1000, 1150, 1300, 1450
		1.375		
		1.625		
		2		
Test 2		2	0	
			33.3	
			66.6	
			90	

Notes: V is the experimental volume of the mudflow, n is the length/width ratio of the boulder, α is the angle between the long axis of the boulder and the flow direction, n is the length/width ratio of the boulder.

2.6. Experimental Procedure

During the testing process, the boulder models are placed in pre-designed positions in the flume, the prepared mudflow is placed into the hopper, and the laser rangefinder and camera are set up and ready for the test to begin. The valve at the hopper outlet is opened, and then a marker ball is quickly placed into the hopper outlet. The mudflow travels through the channel and impacts the boulder. The measurement items and methods used in the test are as follows:

(1) Mudflow velocity: The velocity of the mudflow was obtained by recording the motion of the marker ball in the mudflow using Camera 1.
(2) Variation in mudflow depth. Changes in the mudflow depth during the experiment were recorded using a laser distance-measuring device.
(3) Changes in boulder velocity during boulder initiation. The change in boulder velocity during boulder initiation was recorded using Camera 1. Starting from the instant the mudflow touched the boulder, the change in boulder velocity was recorded every 1/6 s. The average velocity during each period was used as the instantaneous velocity at the next moment to facilitate data processing.
(4) Variation in attitude during boulder movement. Changes in attitude during boulder movement were recorded using Camera 2.
(5) Final movement distance and attitude of the boulder. At the end of the experiment, the final distance moved, and the attitude of the boulders was recorded using a camera.

3. Experimental Result

The movements of the boulders under different conditions showed different patterns. Under different experimental conditions, the movement velocity and depth of the mudflow, as well as the movement velocity and distance of the boulder, were different. Based on the experimental data, the relationship between the boulder's movement distance, movement velocity, movement mode, and each experimental parameter can be analyzed. The experimental data for the mudflow impacting boulders are listed in Table 2.

Table 2. Experimental data.

Test ID	ρ (kg/m^3)	V (m^3)	α (°)	n	v_0 (m/s)	h_m (mm)	v_1 (m/s)	v_2 (m/s)	v_3 (m/s)	v_4 (m/s)	F_r	L (m)
Test 1	1000	0.05	0	1	2.88	21	0.21	0.66	1.02	1.02	6.39	2.59
				1.375	2.64		0.03	0.24	0.54	0.66	5.86	0.875
				1.625	2.76		0	0.18	0.54	0.72	6.12	2.51
				2	2.88		0	0	0	0	6.39	0
	1150	0.05		1	2.64	22.5	0.24	0.84	1.08	1.2	5.66	3.41
				1.375	2.52		0	0.03	0.27	0.66	5.40	2.615
				1.625	2.52		0	0.03	0.24	0.48	5.40	3.17
				2	2.64		0	0	0	0	5.66	0
	1300	0.05		1	2.16	23.5	0.24	0.6	1.02	1.14	4.53	2.965
				1.375	2.16		0.09	0.27	0.54	0.84	4.53	1.255
				1.625	2.28		0.06	0.45	0.72	0.84	4.78	2.6
				2	2.28		0	0	0	0	4.78	0
	1450	0.05		1	2.64	25.5	0.18	0.66	0.9	1.08	5.31	2.765
				1.375	2.88		0.12	0.18	0.48	0.72	5.80	2.53
				1.625	2.64		0.06	0.18	0.48	0.54	5.31	1.89
				2	2.88		0	0	0.06	0.3	5.80	1.98

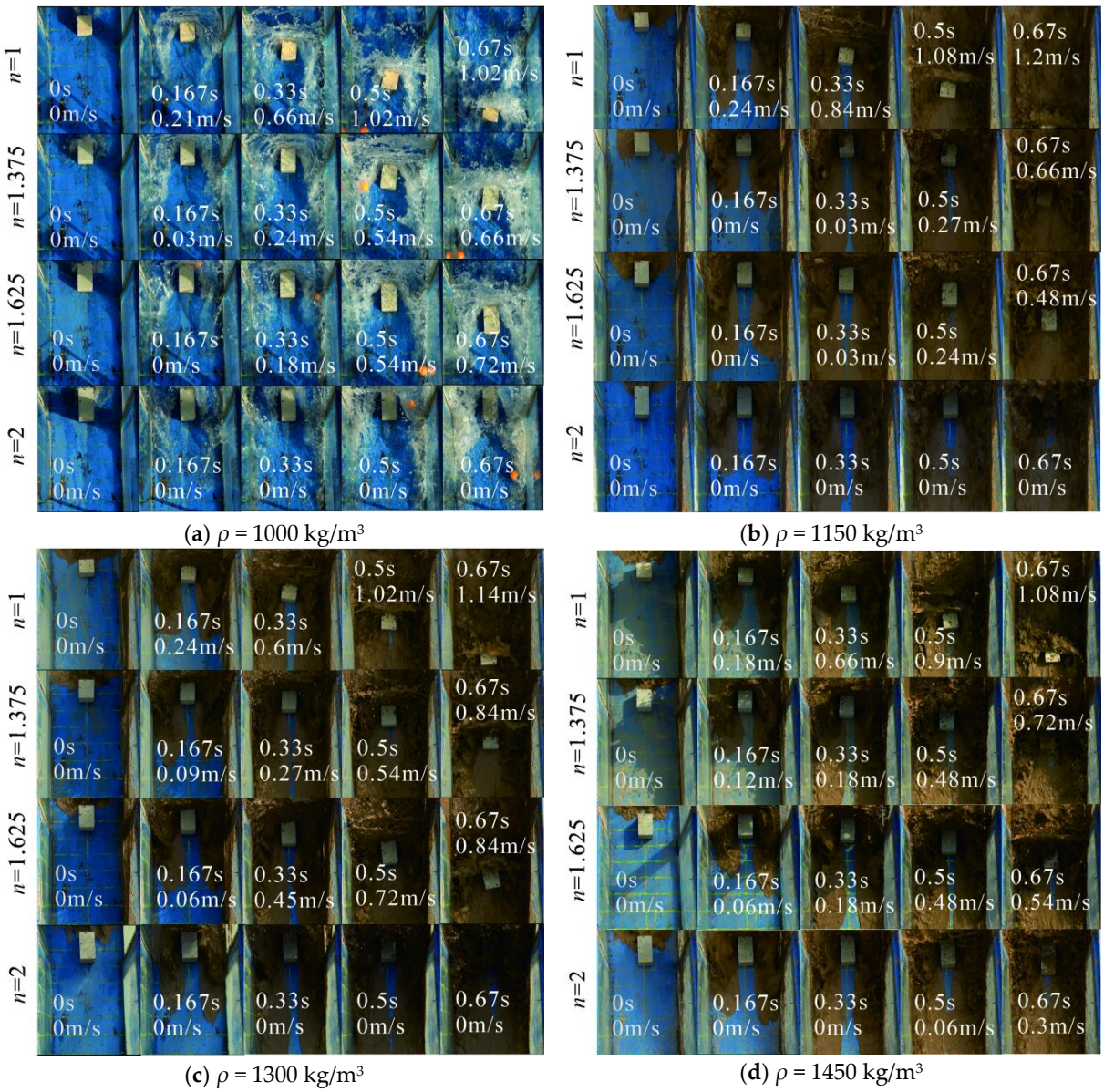
Table 2. *Cont.*

Test ID	ρ (kg/m^3)	V (m^3)	α (°)	n	v_0 (m/s)	h_m (mm)	v_1 (m/s)	v_2 (m/s)	v_3 (m/s)	v_4 (m/s)	F_r	L (m)
Test 2	1000	0.05	0	2	2.88	21	0	0	0	0	6.39	0
			33.3		2.76		0	0.03	0.18	0.3	6.12	0.508
			66.6		2.88		0.18	0.36	0.84	1.08	6.39	1.06
			90		2.76		0.3	0.66	0.96	1.08	6.12	2.166
	1150	0.05	0		2.64	22.5	0	0	0	0	5.66	0
			33.3		2.52		0.03	0.24	0.45	0.6	5.40	0.58
			66.6		2.64		0.18	0.66	1.02	1.14	5.66	2
			90		2.52		0.24	0.78	1.14	1.32	5.40	3.705
	1300	0.05	0		2.28	23.5	0	0	0	0	4.78	0
			33.3		2.16		0.03	0.24	0.54	0.72	4.53	0.61
			66.6		2.16		0.21	0.63	1.02	1.14	4.53	1.37
			90		2.28		0.3	0.84	1.05	1.38	4.78	4.57
	1450	0.05	0		2.88	25.5	0	0	0.06	0.3	5.80	1.98
			33.3		2.88		0	0	0.03	0.27	5.80	0.64
			66.6		2.64		0.12	0.66	0.84	1.07	5.31	1.01
			90		2.88		0.24	0.72	0.96	1.08	5.80	2.285

Notes: ρ represents the density of the mudflow, V is the experimental volume of the mudflow, α is the angle between the long axis of the boulder and the flow direction, n is the length/width ratio of the boulder, v_0 is the velocity of the mudflow, h_m is the maximum depth of the mudflow, v_1, v_2, v_3, v_4 are the velocities of the boulder at each of the four moments. F_r is the Froude number. L is the final distance moved by the boulder.

3.1. Velocity Variation During Boulder Initiation

Figure 7 shows the velocity of the boulder's motion at various moments in Test 1, where the long axis of the boulder was always parallel to the direction of the mudflow. Figure 7 shows that when the long axis of the boulder is parallel to the flow direction, the boulder with a length/width ratio (n) of 2 does not move under the impact of mudflows with densities of 1000 kg/m^3, 1150 kg/m^3, 1300 kg/m^3, and only moves under the scouring of the mudflow with a density of 1450 kg/m^3. However, the boulders did not initiate when they first came into touch with the mudflow but rather between 0.33 and 0.5 s. Three phenomena occurred during the experiment: one in which the boulder was immediately initiated upon touching the mudflow, another in which the boulder was initiated after touching the mudflow, and the other in which the boulder was initiated sometime after touching the mudflow. For example, the experiments with n = 1.625 in Figure 7a, n = 1.375 and 1.625 in Figure 7b, and n = 2 in Figure 7d all belong to the cases where the boulders move after being eroded by mudflow for some time. The movement state of boulders after contact with a mudflow is related to their force state in the mudflow. In Test 2, the boulder initiating but requiring a response time was more likely to occur when the n value was large.

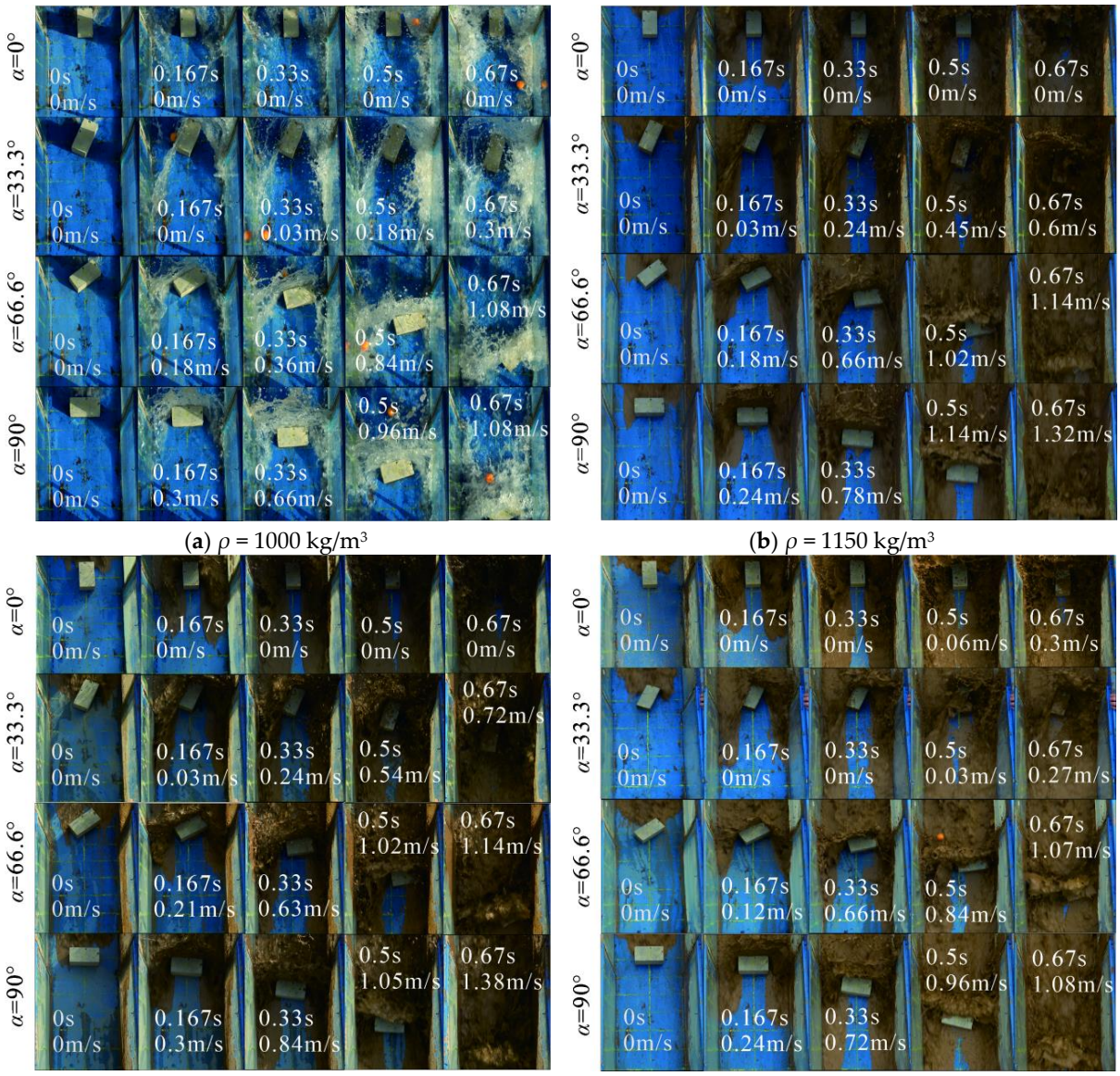


(**a**) ρ = 1000 kg/m^3 (**b**) ρ = 1150 kg/m^3

(**c**) ρ = 1300 kg/m^3 (**d**) ρ = 1450 kg/m^3

Figure 7. Initiation process of boulders with different length/width ratios. ((**a**–**d**) are four different density conditions).

As shown in Figure 8, the motion velocity of the boulder each time in Test 2. In Test 2, the length/width ratio (n) of the boulder was 2. It can be seen from Figure 8 that when the angle between the long axis of the boulder and the direction of the mudflow (α) is 0°, under the impact of the mudflow with densities of 1000 kg/m^3, 1150 kg/m^3, and 1300 kg/m^3, no movement occurs, and only movement occurs under the action of the mudflow with a density of 1450 kg/m^3. However, the boulder did not initiate when it first came into contact with the mudflow but moved within 0.33 to 0.5 s. In Test 2, the boulder initiated but took some response time, such as the test with α of 33.3° in Figure 8a and the tests with α of 0° and 33.3° in Figure 8d. In Test 2, the phenomenon of the boulder initiating but requiring a response time is more likely to occur when the α value is small.



(**a**) ρ = 1000 kg/m^3 (**b**) ρ = 1150 kg/m^3

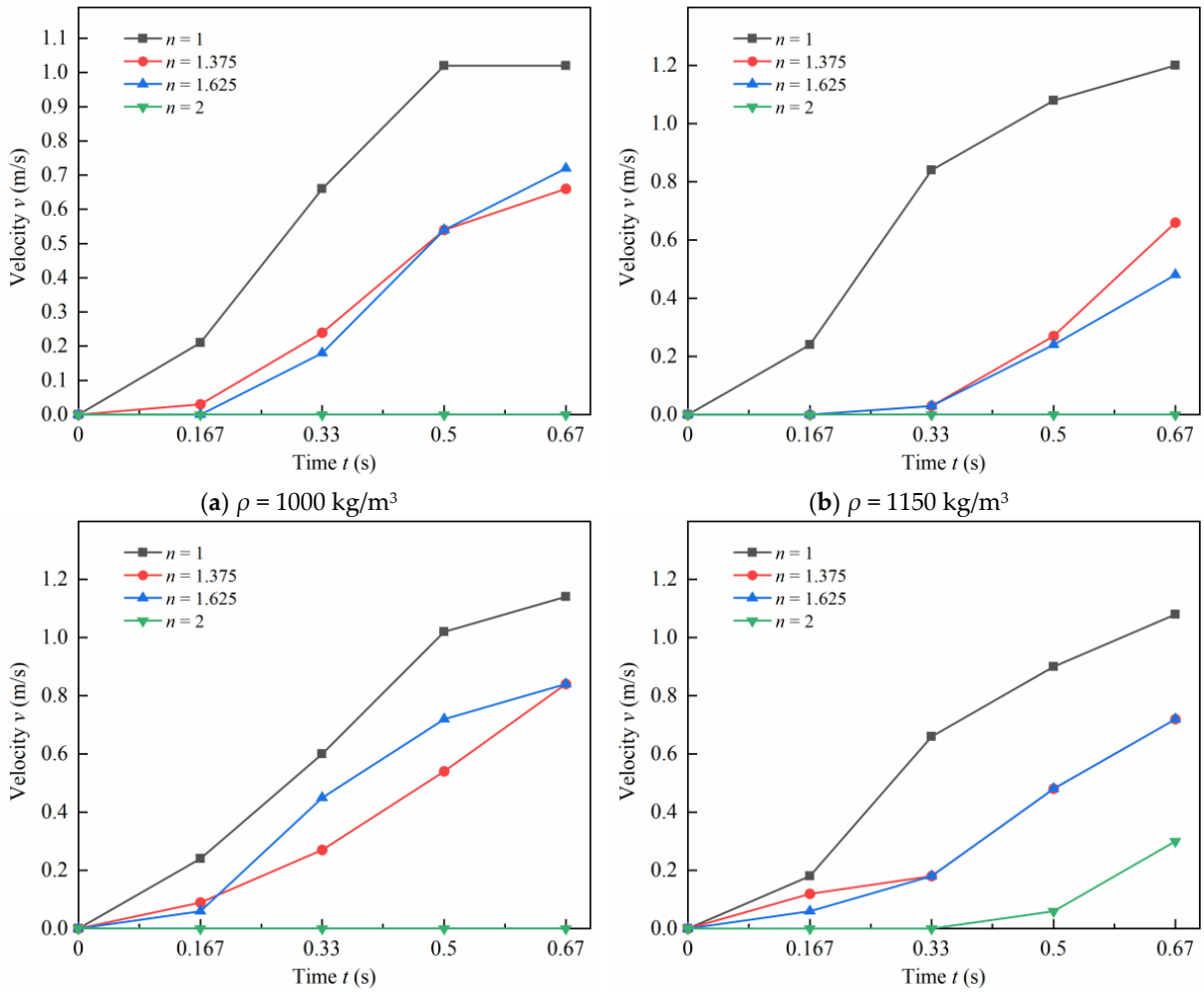
(**c**) ρ = 1300 kg/m^3 (**d**) ρ = 1450 kg/m^3

Figure 8. Initiation process of boulders with different initial angles. ((**a**–**d**) are four different density conditions).

3.2. Initiation Velocity of the Boulder

3.2.1. Effect of Length/Width Ratio on the Initiation Velocity

Figure 9 shows the change in the velocity of boulders with different length/width ratios during initiation in Test 1. It can be observed that the boulder with n = 1 had the largest increase in velocity under the impact of mudflows with different densities, and the boulder with n = 2 had the smallest increase in magnitude. The acceleration stage of the boulders shown in the figure is mainly concentrated within 0 to 0.5 s, while within 0 to 0.167 s, the acceleration of the boulders shown in the figure is relatively small, and within 0.167 to 0.5 s, the acceleration is at the peak value. After 0.5 s, the acceleration of the boulders appears to decrease or be 0. As shown in Figure 9a, the boulder with n of 1 has a relatively small acceleration from 0 to 0.167 s. Within the phase from 0.167 to 0.5 s, the acceleration is at a maximum, and after 0.5 s, the acceleration of the boulder is almost 0.



(**a**) ρ = 1000 kg/m^3 (**b**) ρ = 1150 kg/m^3

(**c**) ρ = 1300 kg/m^3 (**d**) ρ = 1450 kg/m^3

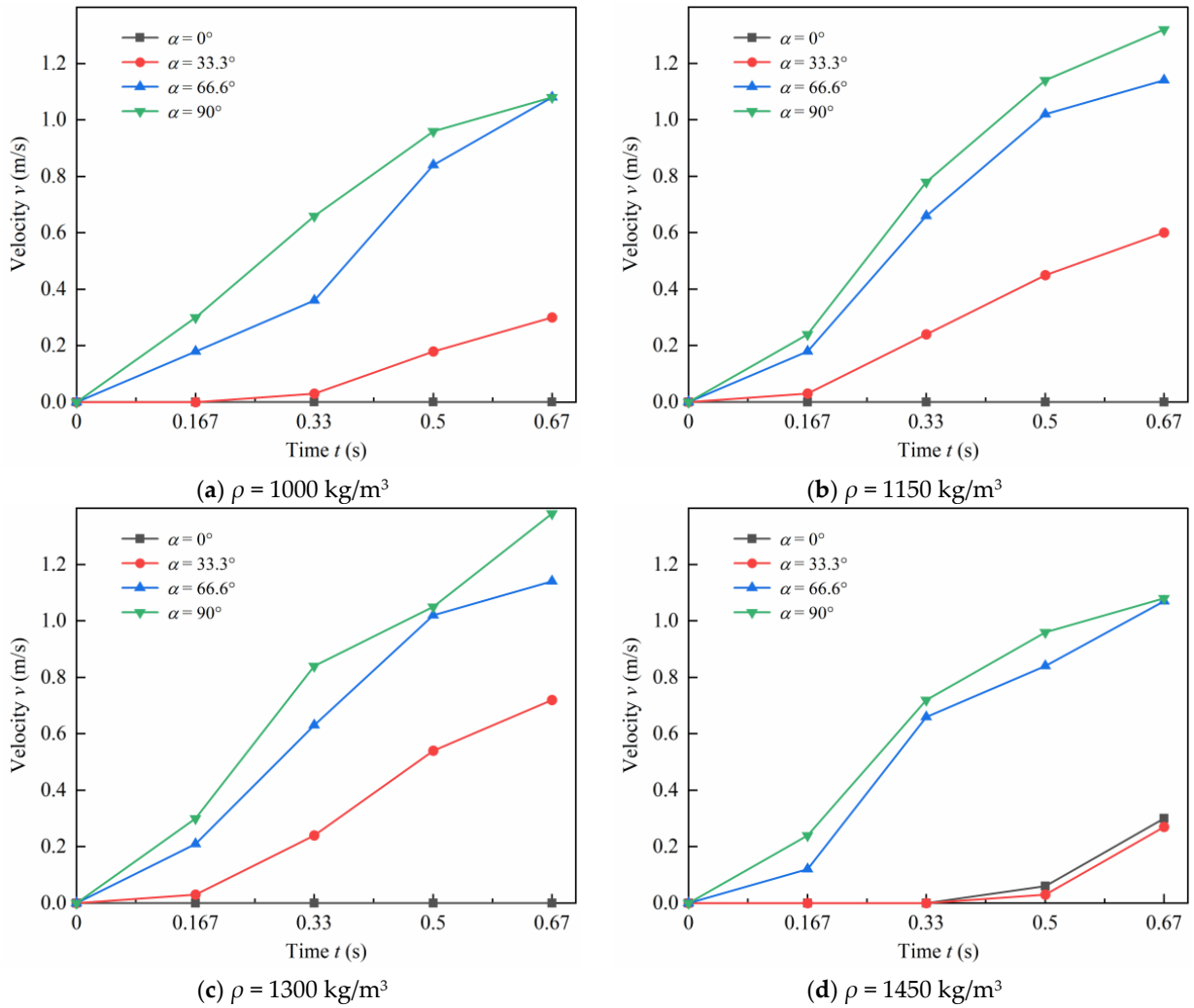
Figure 9. Boulder initiation velocity under different length/width ratio conditions in Test 1. ((**a**–**d**) are four different density conditions).

When the density of the mudflow is larger, the time of decrease in the boulder acceleration shifts relatively later. As shown in Figure 9d, the acceleration of the four boulders in the debris-flow impact at a density of 1450 kg/m^3 did not exhibit a noticeable decreasing trend after 0.5 s. In the boulder initiation process, the velocity of the boulder successively exhibited four stages: slow growth, rapid growth, slow growth, and stabilization. When the long axis of the boulder is parallel to the direction of flow, the larger the length/width ratio of the boulder, the more friction the boulder is subjected to, and the smaller the acceleration and velocity of the boulder during initiation.

3.2.2. Effect of Angle on Initiation Velocity

Figure 10 shows the velocity changes in boulders with different initial positions during the initiation process in Test 2. Similar to the initiation of the boulders in Test 1, the initiation velocity of the boulders in Test 2 successively exhibited four stages: slow growth, fast growth, slow growth, and stabilization. Since the initial position of the long axis of the boulder in Test 1 was parallel to the flow direction, while the long axis of the boulder in Test 2 formed an angle with the flow direction, the angle between the boulder and the flow direction affects the area of action of the drag force of the mudflow on the boulder, which resulted in the area of action of the drag force being generally larger than that of Test 1 in Test 2. So, the acceleration and velocity of the boulder in Test 2 were generally larger than

those in Test 1. As shown in Figure 10, the boulder with α of 90°has the largest increase in velocity, while the boulder with α of 0°has the smallest increase in velocity due to the smallest area of action of the drag force. When the n of the boulder is the same, the larger the α of the boulder, the larger the drag force obtained by the boulder in the startup process, and the larger the startup velocity obtained.



(**a**) ρ = 1000 kg/m^3 (**b**) ρ = 1150 kg/m^3

(**c**) ρ = 1300 kg/m^3 (**d**) ρ = 1450 kg/m^3

Figure 10. Boulder initiation velocity under different angle conditions in Test 2. ((**a**–**d**) are four different density conditions).

3.3. Distance of Boulder Movement

3.3.1. Effect of Length/Width Ratio on the Distance of Boulder Movement

As shown in Figure 11, when the α is 0° and the n is 2, movement occurs only under the action of a mudflow with a density of 1450 kg/m^3. This is because the mass of the boulder with n = 2 is too large, the dragging force produced by the three mudflows with lower densities cannot initiate the boulder, and the area of action of the dragging force does not change.

Boulders with n = 1.375 mostly moved less distance than boulders with n = 1.625 at the same density because the mass of the boulder with n = 1.375 was less than that of the boulder with n = 1.625. The boulders are unevenly impacted by mudflows on both sides of the boulders, which makes them subject to deflection. As the boulder can be activated, the greater the boulder mass, the greater the degree of deflection of the boulder.

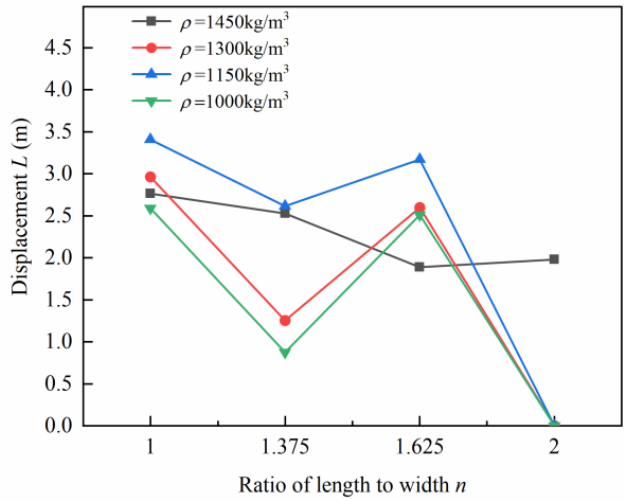


Figure 11. Relationship between the distance of boulder movement and each parameter in Test 1.

3.3.2. Effect of Angle on Distance of Boulder Movement

From Figure 12, it can be seen that there is a clear pattern between the angle between the long axis of the boulder, the flow direction (α), and the boulder movement distance. Whether in floods or under the impact of three different densities of mudflows, the boulder movement distance increases with the increase in α, and the larger the value of α, the larger the increase. This is mainly because the α affects the change of the area of the drag force acting on the boulder by the mudflow. When the size of the boulder was fixed, with an increase in the angle between the long axis of the boulder and the flow direction, the change in the boulder's movement distance gradually increased.

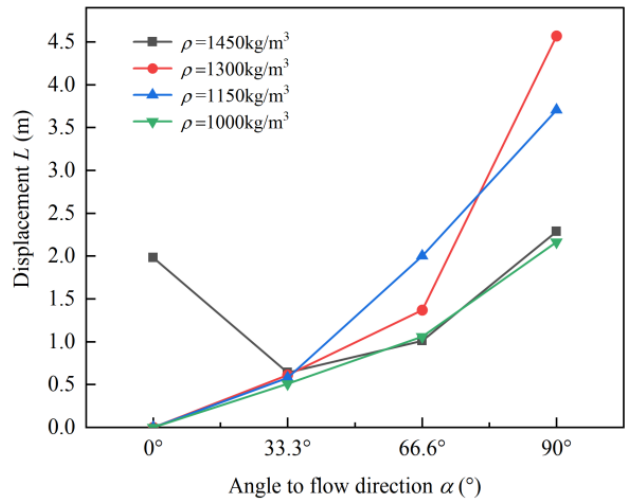
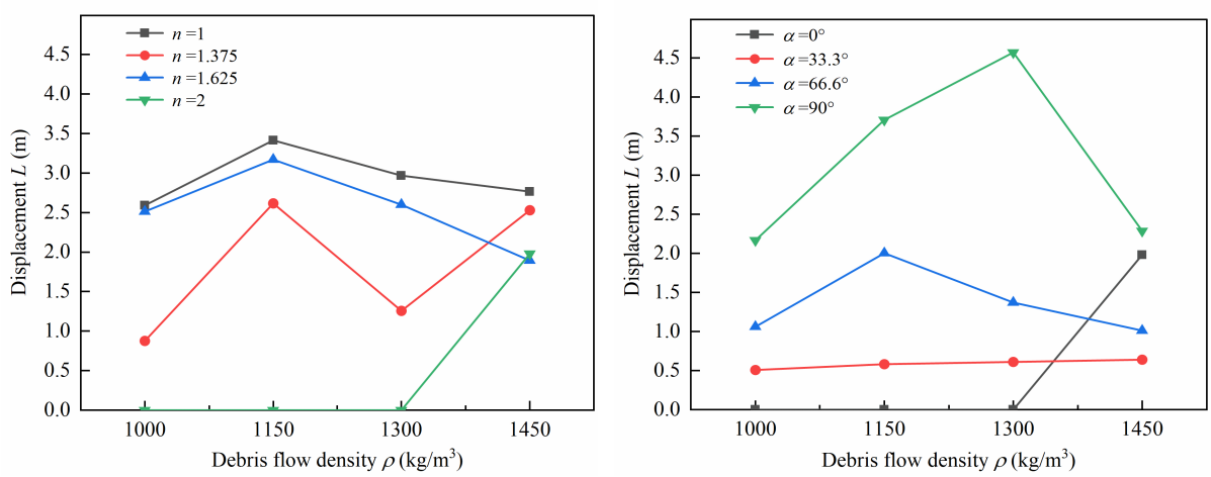


Figure 12. Relationship between the distance of boulder movement and each parameter in Test 2.

3.3.3. The Effect of Mudflow Density on the Distance of Boulder Movement

The difference between a debris-flow impact on a boulder and a tsunami impact on a boulder is that the nature of the mudflow is complex, the velocity of movement of the mudflow is different at different densities, and the impact effect on the boulder is also different. Figure 13 shows the effect of mudflow density on the movement distance of the boulders. As shown in the figure, the movement distance of the boulder first increased and then decreased with an increase in density. Changes in mudflow density involve changes in velocity, mudflow depth, and drag force coefficients, and the situation is highly complex. As shown in Figure 13a, only a mudflow with a density of 1450 kg/m^3 can initiate

a boulder with a long axis parallel to the direction of the flow and an aspect ratio of 2. From Figure 13b, it can be seen that the movement distance of the boulder with n of 2 and α of 33.3° is influenced least by the density of the mudflow.



(**a**) Test 1 (**b**) Test 2

Figure 13. Relationship between boulder movement distance and mudflow density.

3.4. Process of Boulder Movement

In practice, boulders move differently under the impact of mudflows, which is similar to the movement of boulders under the action of tsunamis. Depending on their shape and the forces applied, boulders exhibit three different types of movement: sliding, rolling, and bouncing [24,25]. During the experiment, the boulder was always in a semi-submerged state, and it permanently moved forward in a sliding manner without rolling or bouncing [15]. This is because the mudflow volume was set to be minor, and it was difficult for buoyancy and drag force to be generated by the mudflow under this volume. As shown in Figure 14, a boulder with n of 1 and α of 0° moves under the impact of a mudflow with a density of 1450 kg/m^3, and the boulder only slides and deflects in the process of movement, and no bouncing or rolling phenomenon occurs.

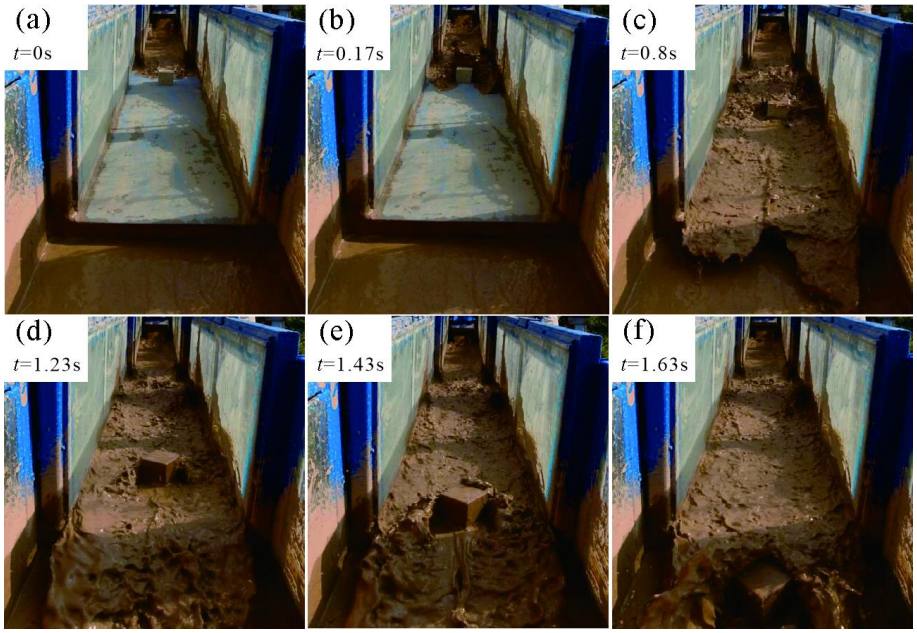


Figure 14. Photos of mudflow impacting boulders. ρ = 1450 kg/m^3, n = 1.

According to the experiment results, it is found that a affects the area of the effective drag force acting on the boulder by the mudflow, which makes the boulder show different deflection tendencies after touching the mudflow, and the different deflection rules will affect the area of the effective drag force acting on the boulder by the mudflow. In the experiments, the boulder, regardless of the initial state, was deflected toward the state in which the long axis was parallel to the flow direction after a certain velocity was obtained during the impact of the mudflow. The movement laws of the boulders are shown in Figure 15.

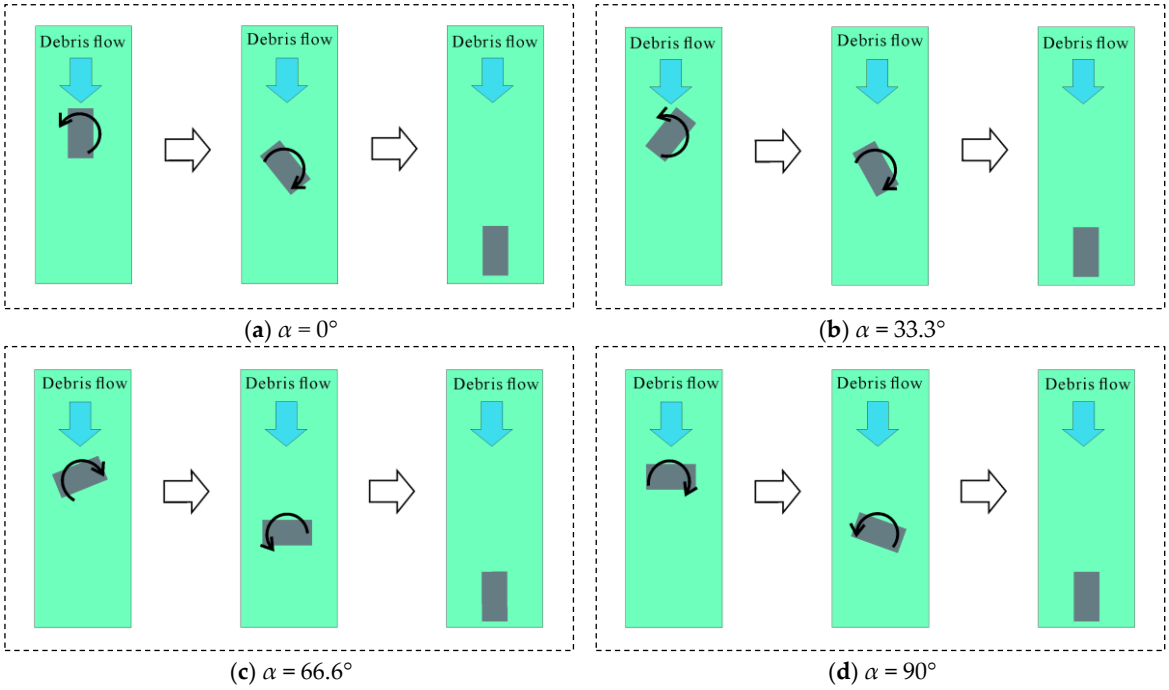


Figure 15. Deflection of boulders by mudflow forces.

Figure 15a shows that a boulder with α of 0°, upon contact with the mudflow, will first be deflected toward a state where the long axis is perpendicular to the direction of the flow and will subsequently move toward a state where the long axis is parallel to the direction of the flow.

Figure 15b shows that the boulder with α of 33.3°, upon contact with the mudflow, will first be deflected toward a state where the long axis is parallel to the flow direction. Then, the long axis of the boulder will be deflected back and forth between the two sides of the flow direction, and the magnitude of the deflection will be larger when the density of the mudflow is larger. Finally, it will be moved toward a state where the long axis is parallel to the flow direction.

Figure 15c shows that the boulder with α of 66.6° will first deflect toward the state where the long axis is perpendicular to the flow direction when it comes in contact with the mudflow and when the boulder moves until the long axis is perpendicular to the flow direction, the boulder will move toward the state where the long axis is parallel to the flow direction.

Figure 15d shows that the boulder with α of 90° will first deflect toward the state with its long axis parallel to the flow direction after contacting the mudflow, and then it will move toward the state with its long axis parallel to the flow direction. When α is 0°and 66.6°, the long axis of the boulder will initially move toward a state perpendicular to the flow direction, increasing the surface facing the flow in order to obtain a larger drag force. This is similar to the movement pattern of boulders under tsunami action [21–25]. It can,

but the deflection tendency is reversed when α is 33.3° and 90°, which may be caused by the difference in the nature of the mudflow and seawater, where the boulders are in different states of stress in the two.

4. Discussion

4.1. Analysis of Boulder Forces

Both domestic and foreign scholars have researched the forces acting on boulders in mudflows [24,39]. The boulders were subjected to different forces in the mudflow and tsunami because the tsunami moved from the low terrain on the far shore to the high terrain on the near shore, while the mudflow moved from the high terrain to the ground terrain in the gully; therefore, the boulders were subjected to the opposite direction of the dragging force in the two cases. Owing to the setting of the debris-flow volume in this experiment, the boulder was in a semi-submerged state. In this experiment, the boulder was subjected to four forces, namely buoyancy, gravity, drag force, and friction, during the impact of the mudflow, and its force state is shown in Figure 16.

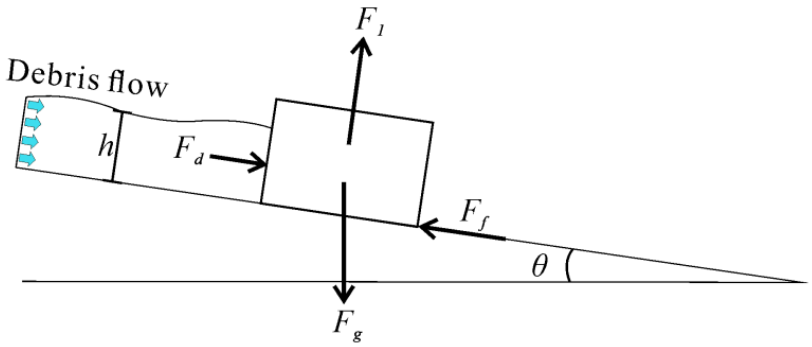


Figure 16. Forces on boulders under the impact of mudflows.

The boulder is subjected to the boulder's gravitational force F_g, the buoyant force F_l exerted on the boulder by the flow, the drag force F_d exerted on the boulder by the flow, and the friction force F_f acting on the contact surface between the boulder and the bottom of the flume in the mudflow, where the formulas for F_g, F_l, F_d, and F_f are as follows:

$$F_g = m_s g \tag{4}$$

$$F_l = \rho_c g V_L \tag{5}$$

$$F_d = \frac{1}{2}\rho_c A_d C_d u^2 \tag{6}$$

$$F_f = \mu(m_s g \cos\theta - \rho_c g V_L) \tag{7}$$

When the boulder just touched the mudflow, it was not surrounded by the mudflow and was not subject to buoyancy. Here, F_f can be expressed as

$$F_f = \mu m_s g \cos\theta \tag{8}$$

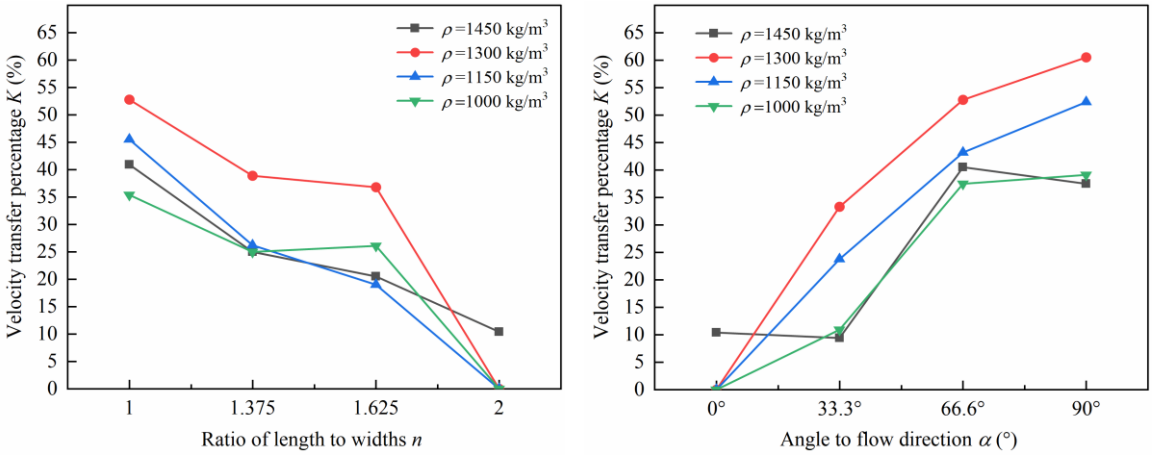
In the formula: m_s is the mass of the boulder (kg); V_L is the volume of the boulder submerged in the slurry; ρ_c is the density of the slurry (kg/m^3); h is the depth of the mudflow (m); u is the effective flow velocity of the mudflow actually acting on the boulder model; ρ_c is the density of the slurry (kg/m^3); A_d is the area of the drag force acting on the surface of the water of the boulder perpendicular to the direction of incoming flow; C_d is the drag force coefficient, which is affected by the shape of the object, the relative position

in the mudslide slurry, and the Reynolds coefficient; μ is the coefficient of friction, which is mainly affected by the boulder morphology and the roughness of the channel.

4.2. Analysis of Boulder Initiation Velocity

From the test results, it can be observed that when the long axis of the boulder is parallel to the flow direction, the larger the n of the boulder, the smaller the acceleration of the boulder in the initiation process, and the smaller the velocity of motion obtained. The density of the boulder is the same; the larger the n, the greater the mass of the boulder. From Equation (7), when the long axis of the boulder is parallel to the flow direction, the effective drag force of the boulder is in the same area, and the smaller the mass of the boulder, the smaller the friction and the greater the velocity. When the n of the boulders are all 2, the larger the α of the boulder, the larger the velocity obtained by the boulder. It can be seen from Equation (6) that the α of the boulder affects the area of the effective drag force acting on the boulder by the mudflow. When α is larger, A_d is larger, and the velocity obtained by the boulder is larger.

In the process of a mudflow impacting a boulder, the maximum instantaneous velocity that the boulder can obtain is different because of differences in the density of the mudflow, the size of the boulder, and other factors. Define K as the ratio of the maximum velocity of the boulder to the velocity of the mudflow, from 0 to 0.67 s. The relationship between the value of K and each parameter for different sets of experiments is shown in Figure 17.



(**a**) Test 1 (**b**) Test 2

Figure 17. Transfer efficiency of boulder velocity.

From Figure 17a, it can be seen that as n increases, the boulder velocity transfer efficiency appears to decrease because boulders with a smaller n are more likely to be deflected in the debris-flow impact, which increases the effective area of action of the drag force and results in a larger drag force and velocity. In Figure 17b, as α increases, K also increases, which is due to the fact that the boulder will first move toward the state where the long axis is perpendicular to the flow direction in the course of all the movements, which increases the effective area of action of the drag force and obtains a larger drag force and initiation velocity. The greater the starting velocity obtained, the higher the velocity transfer efficiency will be.

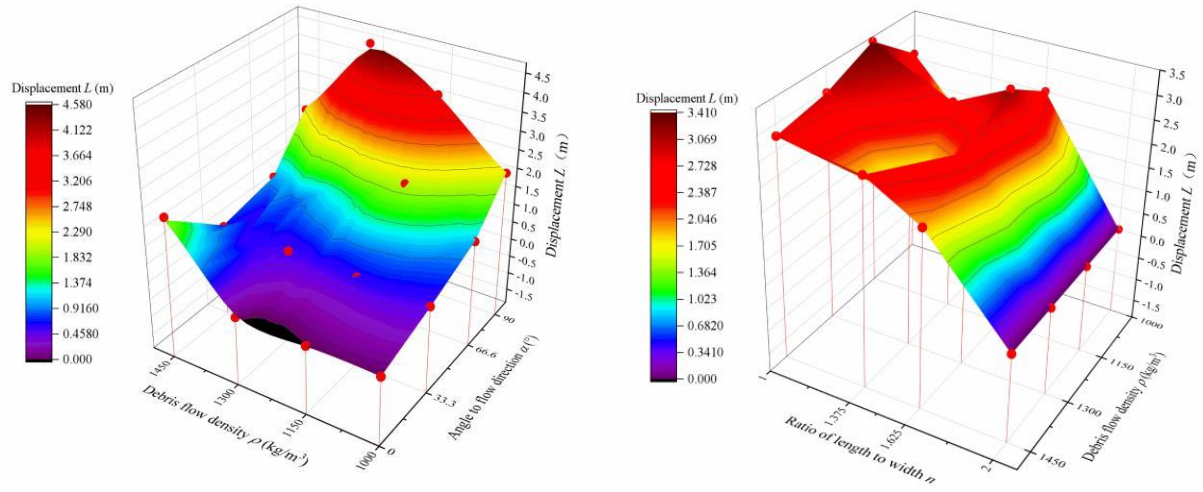
4.3. Analysis of Boulder Movement Distances

The experimental results show that when the long axis of the boulder was parallel to the flow direction, the movement distance of the boulder first decreased, then increased, and then continued to decrease with an increase in n. The movement distance of the boulder

with the n of 1.375 is mostly smaller than that of the boulder with the n of 1.625, which is due to the mass of the boulder with the n of 1.375 being smaller than that of the boulder with the n of 1.625. Both sides of the boulders were deflected due to the uneven impact of the mudflow. Because the drag force has the same area, both types of boulders are subjected to the same effective drag force by the flow, and boulders with n = 1.625 are subjected to greater friction and are deflected more under an uneven impact. The boulder deflection created an area over which the drag force increased, the boulder received a larger drag force and velocity, and the distance traveled increased. A boulder with n = 1.375 is more likely to start owing to the smaller friction, and the inertial force generated by the boulder at the time of initiation reduces the effect of the uneven impact on the boulder, resulting in a smaller boulder deflection, a smaller area of effective drag force, and a smaller distance of movement.

When the size of the boulder is fixed, with the increase in α, the change rule of the boulder movement distance shows a gradual increase. From Equation (6), it can be seen that this is because it will affect the change of the drag force acting area (A_d). With the increase in α, the mudflows on the boulder A_d will also become larger so that the boulder obtains a larger drag force, and the movement distance is farther. α value is larger, the boulder's movement distance is farther, which is the same as the tsunami boulder's movement rules [8,24].

In contrast to boulders under tsunami action, boulders in mudflows are affected by mudflow density, gully slope, gully roughness, and other factors [13,15]. In order to comprehensively consider the effects of ρ, n, and α, the experimental data were organized and analyzed, and the relationship between the final movement distance of the boulder and various experimental parameters was obtained. Figure 18 shows the relationship between the boulder movement distance and ρ, α, and n. From Figure 18a, it can be seen that when the boulder n is 1, the boulder's motion distance is the farthest in the group of tests. When n was 1.375, the motion distance showed a decreasing trend; when n was 1.625, the motion distance increased again, and when n was 2, the motion distance decreased. From Figure 18b, it can be seen that when the α is 90°, the movement distance of the boulder is the farthest in this group of tests. From the figure, it can be seen that the correlation between the boulder movement distance, boulder length/width ratio, and angle between the long axis and flow direction is stronger.



(**a**) Test 1 (**b**) Test 2

Figure 18. Integrated relationship between boulder movement distance and each parameter.

4.4. Initiation Conditions for Boulders

As shown in Figure 19, the experiment showed that boulders with the same initial position were partially displaced and partially remained stationary at all times under the impact of four different mudflow densities. A boulder with a length/width ratio of 2 was placed in the flume in the same state as the mudflow direction; it was not displaced under the impact of the mudflow with densities of 1150 kg/m^3 and 1300 kg/m^3 as well as under the impact of the water flow, and was only displaced under the impact of the mudflow with a density of 1450 kg/m^3.

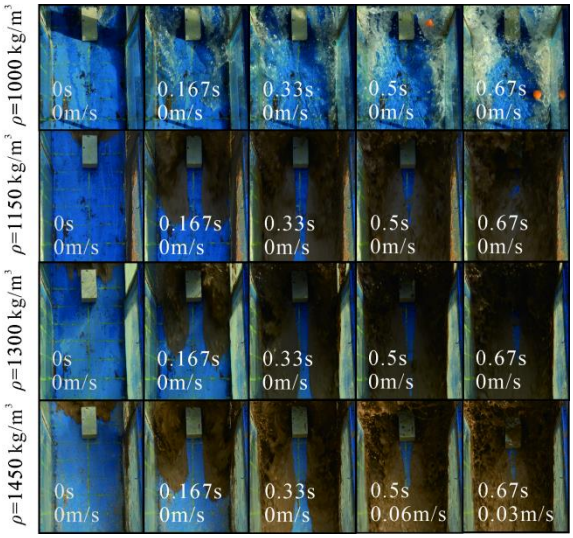


Figure 19. Velocity variation of the boulder initiation process. $n = 2$, $\alpha = 0°$.

When this boulder was impacted by a mudflow with a density of 1450 kg/m^3, the movement was not generated at the moment of contact with the mudflow, but the velocity only changed by 0.5 s. This is because at the beginning of the mudflow, the velocity and flow depth are unstable, and the dragging force of the mudflow alone cannot make the boulder move. During the mudflow, the stone was gradually surrounded by the mudflow in a semi-submerged manner. Under buoyancy, the drag force on the boulder gradually became greater than the friction force experienced by the boulder, and the boulder began to move under the influence of the dragging force.

As shown in Figure 16, the initiation condition of the boulder is

$$F_d + F_g \sin\theta \geq F_f \tag{9}$$

The force state of the boulder in the mudflow is different from the force under the action of the tsunami on the boulder. The boulder in seawater is always under the action of buoyancy, whereas in the process of mudflow impact, the boulder will only be under the action of buoyancy when it is surrounded. Therefore, when the mudflow comes into contact with a boulder, the boulder does not receive the buoyancy produced by the mudflow, and F_f is expressed as Equations (8) and (9) and can be written as

$$\frac{1}{2}\rho_c A_d C_d u^2 + m_s g \sin\theta \geq \mu m_s g \cos\theta \tag{10}$$

When the mudflow touches a boulder, it is initiated under the following condition:

$$u^2 \geq \frac{2m_s g(\mu\cos\theta - \sin\theta)}{\rho_c A_d C_d} \tag{11}$$

A mudflow surrounded the boulder. The boulder is subjected to buoyancy, F_f is expressed by Equations (7) and (9) can be written as

$$\frac{1}{2}\rho_c A_d C_d u^2 + m_s g \sin\theta \geq \mu(m_s g \cos\theta - \rho_c g V_L) \tag{12}$$

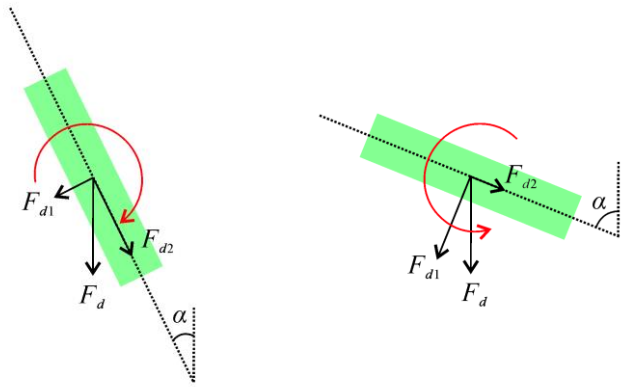
When a boulder is surrounded by mudflow, it is subjected to buoyancy, which is the starting condition for the boulder.

$$u^2 \geq \frac{2m_s g(\mu\cos\theta - \sin\theta) - 2\mu\rho_c g V_L}{\rho_c A_d C_d} \tag{13}$$

4.5. Principle of Deflection of Boulders

The initial position of a boulder in a gully affects its velocity, distance of movement, force, and deposition position under the impact of a mudflow. This is closely related to the prevention and control of mudflow disasters in mountainous areas.

There were four different values set for the angle between the long axis of the boulder and the flow direction (α) in the experiment, and according to the experiment results and Figure 15, it can be seen that when the α is 33.3° the boulder will be first deflected toward the state in which the long axis is parallel to the flow direction, whereas when the α is 66.6°, the boulder's long axis will be first deflected toward the state in which the boulder is perpendicular to the flow direction. As shown in Figure 20, the boulder deflection is due to the fact that the angle between the long axis of the boulder and the flow direction (α) affects the drag force on the boulder, as shown in Figure 20a, when $\alpha < 45°$, the drag force F_d on the boulder generated by the mudflow in the direction perpendicular to the long axis, F_{d1}, is smaller than the drag force in the direction of the long axis, F_{d2}, which causes the boulder to deflect toward a state where the long axis is parallel to the flow direction. As shown in Figure 20b, when $\alpha > 45°$, the drag force F_{d1} generated by the mudflow on the boulder in the direction perpendicular to the long axis is larger than the drag force F_{d2} in the direction of the long axis, causing the boulder to be deflected toward the state in which the long axis is perpendicular to the flow direction.



(**a**) $\alpha < 45°$ (**b**) $\alpha > 45°$

Figure 20. Schematic of the force deflection of the boulder.

5. Conclusions

This study mainly focuses on the impact motion process of mudflows on boulders. In this study, we designed a flume model experiment for mudflows impacting rectangular boulders. By impacting boulders of different sizes with mudflows of different densities, the impact of the mudflow density, the length/width ratio of the boulders, and the an-

gle between the long axis and flow direction on the starting velocity, displacement, and movement state of the boulders were analyzed. The following conclusions were drawn:

(1) During the impact process of the mudflow on the boulders, the long axis of the boulder deflects under the uneven impact of the mudflow on both sides, increasing the area of the acting drag force and obtaining a more significant drag force. When the initial long axis of the boulder is parallel to the flow direction, the smaller the mass of the boulder, the less likely it is to deflect. However, when the boulder can be started, the difference between the drag force and the friction force is small, and the deflection of the boulder is obvious.

(2) The velocity during the boulder movement successively exhibited four stages: slow growth, rapid growth, slow growth, and stabilization. In the test, the acceleration of the boulder stabilized at a lower value from 0 to 0.167 s, stabilized at the peak state from 0.167 s to 0.5 s, and then entered into the acceleration decrease stage. When the long axis of the boulder is parallel to the flow direction, the smaller the boulder mass, the greater the transfer efficiency of the mudflow on the boulder velocity. When an angle exists between the long axis of the boulder and the flow direction, the larger the angle, the larger the drag force area and velocity transfer efficiency.

(3) The difference between the boulder force in the mudflow and tsunami was that the boulder in the seawater was always buoyant, whereas the boulder was buoyant only when the mudflow surrounded it, and the direction of the drag force of the boulder was different in the two cases.

Author Contributions: Conceptualization, R.L. and C.L.; methodology, F.W.; software, R.L.; formal analysis, R.L.; resources, X.C. and H.Q.; writing—original draft preparation, R.L.; writing—review and editing, F.W.; funding acquisition, J.W. All authors have read and agreed to the published version of the manuscript.

Funding: This research was funded by The National Natural Science Foundation of China, grant number 41807252.

Institutional Review Board Statement: Not applicable.

Informed Consent Statement: Not applicable.

Data Availability Statement: The authors agree to make data supporting the results or analyses presented in this paper available upon reasonable request from the first author and corresponding author.

Acknowledgments: We are grateful for the support of the debris flow simulation test platform of the Department of Geology, Northwest University, China.

Conflicts of Interest: The authors declare no conflicts of interest.

References

1. Fu, W.X.; Nie, D.X.; Ren, G.M.; Chen, H.J.; Wan, Z.L.; Yang, T.J.; Zhang, F.R. The Study on Debris Flow's Distribution Regularity in China. *Chin. J. Geol. Hazard Control* **1997**, *4*, 40–44. (In Chinese)
2. Iverson RM The physics of debris flows. *Rev. Geophys.* **1997**, *35*, 245–296. [CrossRef]
3. Cui, P.; Zhuang, J.Q.; Chen, X.C.; Zhang, J.Q.; Zhou, X.J. Characteristics and countermeasures of debris flow in Wenchuan area after the earthquake. *J. Sichuan Univ. (Eng. Sci. Ed.)* **2010**, *42*, 10–19.
4. Hu, G.S.; Chen, N.S.; Deng, M.F.; Lu, Y. Analysis of the Characteristics of Impact Force of Massive Stones of the Sanyanyu Debris Flow Gully in Zhouqu, Gansu Province. *Earth Environ.* **2011**, *4*, 478–484. [CrossRef]
5. Wang, F.; Chen, X.Q.; Li, Y.; Li, K.; Yu, X.B. Fluid-solid Coupling Analysis of Boulder Rolling in Channel after Silt Dam Filled Based on Flow-3d. *Sci. Technol. Eng.* **2015**, *15*, 14–20. (In Chinese)
6. Bugnion, L.; Mcardell, B.W.; Bartelt, P.; Wendeler, C. Measurements of hillslope debris flow impact pressure on obstacles. *Landslides* **2012**, *9*, 179–187. [CrossRef]
7. Choi, C.E.; Ng, C.W.; Song, D.; Kwan, J.S.; Shiu, H.Y.; Ho, K.K.; Koo, R.C. Corrigendum: Flume investigation of landslide debris-resisting baffles. *Can. Geotech. J.* **2014**, *51*, 255. [CrossRef]

8. Petroff, C.; Moore, A.; Arnason, H. Particle advection by turbulent bores—Orientation effects. In Proceedings of the International Tsunami Symposium, Seattle, WA, USA, 7–10 August 2001.
9. Wang, D.; Chen, Z.; He, S.; Liu, Y.; Tang, H. Measuring and estimating the impact pressure of debris flows on bridge piers based on large-scale laboratory experiments. *Landslides* **2018**, *15*, 1331–1345. [CrossRef]
10. Xu, Y.H.; Zhang, W.S.; Zhao, Y.X.; Wang, S.L. Numerical simulation of large particles moving in debris flow. *J. Hydraul. Eng.* **2012**, *S2*, 98–104. (In Chinese) [CrossRef]
11. Tang, B.H.; Sun, H.Y. Relationships between starting motion of large-sized particles in debris flow and water flow condition. *J. Nat. Disasters* **2017**, *3*, 132–138. (In Chinese) [CrossRef]
12. Tang, B.H.; Sun, H.Y.; Hu, H.H. Analysis on critical hydraulic condition for starting motion of large-sized particles in viscous debris flow. *J. Eng. Geol.* **2018**, *26*, 1631–1637. (In Chinese) [CrossRef]
13. Si, G.W.; Chen, X.Q.; Chen, J.G.; Tang, J.B.; Zhao, W.Y.; Jin, K. The Impact Force of Large Boulders with Irregular Shape in Flash Flood and Debris Flow. *KSCE J. Civ. Eng.* **2022**, *26*, 4276–4289. [CrossRef]
14. Vicari, H.; Tran, Q.A.; Nordal, S.; Thakur, V. MPM modelling of debris flow entrainment and interaction with an upstream flexible barrier. *Landslides* **2022**, *19*, 2101–2115. [CrossRef]
15. Wang, F.; Wang, J.; Chen, X.; Zhang, S.; Qiu, H.; Lou, C. Numerical Simulation of Boulder Fluid–Solid Coupling in Debris Flow: A Case Study in Zhouqu County, Gansu Province, China. *Water* **2022**, *14*, 3884. [CrossRef]
16. Sha, S.; Dyson, A.P.; Kefayati, G.; Tolooiyan, A. Modelling of debris flow-boulder-barrier interactions using the Coupled Eulerian Lagrangian method. *Appl. Math. Modell.* **2024**, *127*, 143–171. [CrossRef]
17. Nott, J. Extremely high-energy wave deposits inside the Great Barrier Reef, Australia: Determining the cause—Tsunami or tropical cyclone. *Mar. Geol.* **1997**, *141*, 193–207. [CrossRef]
18. Nott, J. Waves, coastal boulder deposits and the importance of the pre-transport setting. *Earth Planet. Sci. Lett.* **2003**, *210*, 269–276. [CrossRef]
19. Goto, K.; Okada, K.; Imamura, F. Numerical analysis of boulder transport by the 2004 Indian Ocean tsunami at Pakarang Cape, Thailand. *Mar. Geol.* **2010**, *268*, 97–105. [CrossRef]
20. Paris, R.; Fournier, J.; Poizot, E.; Etienne, S.; Morin, J.; Lavigne, F.; Wassmer, P. Boulder and fine sediment transport and deposition by the 2004 tsunami in Lhok Nga (western Banda Aceh, Sumatra, Indonesia): A coupled offshore–onshore model. *Mar. Geol.* **2010**, *268*, 43–54. [CrossRef]
21. Nandasena, N.A.K.; Tanaka, N. Boulder transport by high energy: Numerical model-fitting experimental observations. *Ocean Eng.* **2013**, *57*, 163–179. [CrossRef]
22. Zainali, A.; Weiss, R. Boulder dislodgement and transport by solitary waves: Insights from three-dimensional numerical simulations. *Geophys. Res. Lett.* **2015**, *42*, 4490–4497. [CrossRef]
23. Gandhi, D.; Chavare, K.A.; Prizomwala, S.P.; Bhatt, N.; Bhatt, N.Y.; Mohan, K.; Rastogi, B.K. Testing the numerical models for boulder transport through high energy marine wave event: An example from southern Saurashtra, western India. *Quat. Int.* **2017**, *444*, 209–216. [CrossRef]
24. Imamura, F.; Goto, K.; Ohkubo, S. A numerical model for the transport of a boulder by tsunami. *J. Geophys. Res.* **2008**, *113*, 2007JC004170. [CrossRef]
25. Bressan, L.; Guerrero, M.; Antonini, A.; Petruzzelli, V.; Archetti, R.; Lamberti, A.; Tinti, S. A laboratory experiment on the incipient motion of boulders by high-energy coastal flows. *Earth Surf. Processes Landforms.* **2018**, *43*, 2935–2947. [CrossRef]
26. Liu, H.; Sakashita, T.; Sato, S. An experimental study on the tsunami boulder movement. In Proceedings of the 34th International Conference on Coastal Engineering, Seoul, Republic of Korea, 15–20 June 2014. [CrossRef]
27. Oetjen, J.; Engel, M.; Bruckner, H.; Pudasaini, S.P.; Schuttrumpf, H. Enhanced Field Observation Based Physical and Numerical Modelling of Tsunami Induced Boulder Transport Phase 1: Physical Experiments. *Int. Conf. Coast. Eng.* **2017**, *1*, 4. [CrossRef]
28. Oetjen, J.; Engel, M.; Pudasaini, S.P.; Schuettrumpf, H. Significance of boulder shape, shoreline configuration and pre-transport setting for the transport of boulders by tsunamis. *Earth Surf. Process. Landforms.* **2020**, *45*, 2118–2133. [CrossRef]
29. Xiao, X.W.; Xia, J.Q.; Shu, C.W.; Chen, Y.M. Theoretical analysis and experimental study of stability of flooded vehicles. *J. Sediment Res.* **2013**, *1*, 53–59. (In Chinese) [CrossRef]
30. Shu, C.W.; Xia, J.Q.; Lin, B.L.; Tan, G.M. Estimation of Incipient Velocity of Flooded Vehicles. *J. Catastrophol.* **2012**, *1*, 28–33+43. (In Chinese)
31. Shu, C.W.; Chen, X.D.; Kong, W.N. Experimental study of man-vehicle towing forces in floods. In Proceedings of the China Water Resources Society 2018 Annual Academic Conference Proceedings, Division 3, New Orleans, LA, USA, 29 September–3 October 2018; pp. 302–308. (In Chinese). [CrossRef]
32. Cailleux, A.; Tricart, J. *Contribution a L'etude Des Sables Et Des Galets*; CDU: Paris, France, 1959; 376p.
33. Li, P.; Wang, J.; Hu, K.; Shen, F. Effects of bed longitudinal inflexion and sediment porosity on basal entrainment mechanism: Insights from laboratory debris flows. *Landslides* **2021**, *18*, 3041–3062. [CrossRef]
34. Iverson, R.M. Scaling and design of landslide and debris-flow experiments. *Geomorphology* **2015**, *244*, 9–20. [CrossRef]

35. Lanzoni, S.; Gregoretti, C.; Stancanelli, L.M. Coarse-grained debris flow dynamics on erodible beds. *JGR Earth Surf.* **2017**, *122*, 592–614. [CrossRef]
36. Xie, T.; Yang, H.; Wei, F.; Gardner, J.S.; Dai, Z.; Xie, X. A new water–sediment separation structure for debris flow defense and its model test. *Bull. Eng. Geol. Environ.* **2014**, *73*, 947–958. [CrossRef]
37. Wang, D.P.; Chen, Z.; He, S.M.; Chen, K.J.; Liu, F.M.; Li, M.Q. Physical model experiments of dynamic interaction between debris flow and bridge pier model. *Rock Soil Mech.* **2019**, *9*, 3363–3372. (In Chinese) [CrossRef]
38. Li, S.; Wang, J.; Wang, F.; Li, P. Experimental study on a debris flow water-sediment separation structure of a funnel-type grating and its sorting characteristics. *Bull. Eng. Geol. Environ.* **2023**, *82*, 148. [CrossRef]
39. Lodhi, H.A.; Hasan, H.; Nandasena, N.A.K. The role of hydrodynamic impact force in subaerial boulder transport by tsunami—Experimental evidence and revision of boulder transport equation. *Sediment. Geol.* **2020**, *408*, 105745. [CrossRef]

Disclaimer/Publisher's Note: The statements, opinions and data contained in all publications are solely those of the individual author(s) and contributor(s) and not of MDPI and/or the editor(s). MDPI and/or the editor(s) disclaim responsibility for any injury to people or property resulting from any ideas, methods, instructions or products referred to in the content.